RSC Advances

ROYAL SOCIETY OF CHEMISTRY

www.rsc.org/advances

Periodic DFT Study of Donor Interactions with the $MgCl_2$ Surface in the Ziegler-Natta Catalytic System

Kefeng Xie[a,b], Bochao Zhu[b], Renwei Xu[b], Jingcheng Xu[c], Peng Liu[a,*]

[a]College of Chemistry and Chemical Engineering, Lanzhou University, Lanzhou, 730000, China

[b]Lanzhou Petrochemical Research Center, Petrochina, Lanzhou, 730060, China

[c]School of Materials Science and Engineering, University of Shanghai for Science and Technology, Shanghai, 200093, China

Email: pliu@lzu.edu.cn

Abstract: Using periodic DFT, the present study evaluated the interactions of donors with $MgCl_2$ surfaces. The selected donors included 1,3-dimethoxy-2,2-dimethylpropane, dimethoxydimethylsilane, and dimethyl phthalate. The absorption energies and distances of Mg-O were obtained from α-$MgCl_2$ (110), (100), and β-$MgCl_2$ (110), (100), and (104) surfaces. Donors on α and β-$MgCl_2$ (110) surfaces reflected the largest absorption energies among the complexes examined. Results indicated that the surface of $MgCl_2$ was controlled by choosing an appropriate choice of electron donor. Findings indicated that control of the $MgCl_2$ surface may be achieved by selecting an appropriate electron donor. The results of the present work indicate that control of the $MgCl_2$ surface was attainable by appropriate selection of an electron donor; such a concept was utilizable in heterogeneous Ziegler–Natta olefin polymerization catalysis.

Keywords: donor, $MgCl_2$, coordinated, periodic DFT.

1. Introduction

Ziegler-Natta (Z-N) catalysts for olefin polymerization were among the most important discoveries in chemistry. Formation of the active catalyst occurred in several steps and involves a $MgCl_2$ support to which $TiCl_4$ and a Lewis base were added. Lewis bases can be added during catalyst preparation (internal donor, ID) or

olefin polymerization (external donor) [1]. The ID increased catalyst stereoselectivity drastically [2], exerted a significant influence on catalyst regioselectivity, influenced hydrogen responses [3], and modified active site distribution [4, 5]. Development of the Z-N polymerization process involved five generations of catalysts in which electron donors performed a crucial function [6]. In particular, the fourth generation of catalysts, which included phthalate as an ID and organic siloxane as the external donor, had been successfully applied to produce highly isotactic polypropylenes. Since the development of the fourth generation of catalysts, several studies on electron donors had been carried out [1]. IDs such as 1,3-diether, phthalate esters, succinate, malonicester, 1,3-diol ester, glutaric acid ester, 1,3-dione, diamine, isocyanate, cycloalkyl ester, and 1,4-diol had been developed, and catalysts using succinate and 1,3-diether as the ID had been commercialized [7].

Although Z–N catalysis had been studied since 1953, investigations of the molecular level of the catalyst structure, the micro-kinetic mechanistic reaction paths, and the macro-kinetic reaction engineering level of the total polymerization process remained popular research topics to this day [8]. To better understand complex systems consisting of multiple components interacting with one another, understanding the physicochemical properties of each component and allowing them to interact together with increasing complexity were necessary [9]. Several groups recently addressed the question by means of quantum mechanics (QM) and obtained unexpected and often-puzzling results. The interplay between the $TiCl_4$-ID, $MgCl_2$-$TiCl_4$, and $MgCl_2$-ID interactions can significantly modulate the performance of $MgCl_2$-supported Z-N catalysis. A periodic density functional theory (DFT) that is one of the most frequently used computational tools of QM studied on the bulk and surface structures of $MgCl_2$ intended to provide a well-defined picture of the support [10–12]. As a catalyst carrier, $MgCl_2$ formed catalytically active species via binding other catalyst components, titanium chlorides and electron-donating compounds in particular [13, 14]. The microstructure of $MgCl_2$ crystallites was controlled by electron donors; control of catalytic behavior can be achieved by varying the relative proportions of (100) and (110) surface sites [15]. The location of donors in the

vicinity of active sites was a prerequisite for the formation of isospecific active sites: the donor converted an aspecific site into an isospecific one by creating a suitable chiral environment [16]. Two strategies were employed to explain the stereoregulating ability of ID. The first postulated that ID directly participated in stereoregulation by coordinating with active centers (Ti atoms) [17, 18] or to the $MgCl_2$ surface not far from Ti species, thereby turning aspecific Ti species into stereospecific ones [19]. The second strategy presumed the oblique role of ID in stereocontrol. Although studies on this topic had provided significant knowledge on the structure of isospecific active sites and the role of donors, complete agreement on relevant issues had not been achieved because the stability of the active site remained controversial and definite evidence of the presence or absence of donors in the neighborhood of isospecific active sites had not been reported. DFT-based theoretical calculations had recently proven to be useful for rationalizing a number of empirical observations on polymerization reactions using Z-N catalysts [17, 20–25]. Periodic DFT had been used by D'Amore [26] to study the adsorption of small model silane on the surfaces of α-$MgCl_2$. Gupta's group [23] studied phthalates and alkoxy benzoates to stabilize the $MgCl_2$ support through the zip mode of coordination using DFT.

In this paper, we carried out a periodic DFT investigation to improve the current understanding on the functions of internal and external donors by focusing on the relative stabilities of the complexes formed by the donors when coordinated to α and β phases of $MgCl_2$. Two internal donor families – 1,3-diether and phthalate esters, and one external family – alkoxysilane were considered in this study. The present work represented the next step in our systematic approach to exploring the mechanistic aspects of propylene polymerization by Z-N catalysts. Specifically, we investigated the functions of 1,3-dimethoxy-2,2-dimethylpropane, dimethoxydimethylsilane, and dimethyl phthalate as electron donors for tuning the regio- and stereo-selective preferences of propylene polymerization.

2. Computational details

In the thermodynamically most stable α-form the Cl-Mg-Cl triple layers repeated in an ABCABC... sequence (Fig. 1a). Other known structures were the β-forms which

had an AAA... repeating sequence (Fig.1c); here, Mg filled all octahedral cavities between two closely packed Cl planes. Several α-$MgCl_2$ and β-$MgCl_2$ surfaces were selected to achieve a detailed examination based on earlier experimental and theoretical literature. To define 2-D slab models, the following automated procedure was adopted: A 3-D model of the crystallographic structure conforming to the standard database was built in Material Studio. The α-phase crystal was trigonal and of the space group R-3M with a = b = 3.6363Å and c = 17.66629Å, while the β-phase crystal was trigonal and of the space group P-3M1 with a = b = 3.641Å and c = 5.927Å. Slab models, i.e., 3-D objects, that were periodic in two dimensions were then built parallel to the given crystallographic (hkl) plane. Periodic DFT calculations were performed on $MgCl_2$ slabs (2-D periodicity) using the $Dmol^3$ software in the Materials Studio package [27, 28]. All the geometries had been obtained using hybrid density functional method PWC of local-density approximation (LDA-PWC) with dispersion forces [29] duo to consider van der Waals force. Localized double numerical basis sets with polarization functions (DNP) were used to expand the Kohn–Sham orbitals, and periodic boundary conditions were employed to simulate infinite $MgCl_2$ slabs (Figure 1). A vacuum space of 15 Å was applied in the direction normal to the $MgCl_2$ slabs to avoid interactions between two layers. In all cases, the reciprocal space was represented by the Monkhorst–Pack special k-point scheme [30] with 5×5×1 grid meshes. During the geometry optimization, the whole of the system was relaxed. Criteria of convergences of energy, force, and displacement were set as 1×10^{-5} Ha, 0.001 Ha/Å, and 0.005Å, respectively. Moreover, the 6-31G(d,p) basis set in Gaussian 03 was adopted to verify the results of LDA-PWC in $Dmol^3$ by bulk of $MgCl_2$. Donor coverage was an important factor controlling the relative stability of surfaces with an impact on the $TiCl_4$ adsorption process. DMDP, DMDS and DMP (Figure 2) were selected as donors in this study. We defined the donor adsorption energy ΔE according to Equation 1:

$$\Delta E = E_{MgCl_2/donor} - E_{MgCl_2} - E_{donor} \quad (1)$$

where $E_{MgCl_2/donor}$ was the energy of the system composed of the adsorbed donor

and the $MgCl_2$ surface and E_{MgCl_2} and E_{donor} were the respective energies of the uncovered $MgCl_2$ system and the donor in the cell.

3. Results and Discussion

3.1 The selection of basis set.

The Mg atom on the surface of $MgCl_2$ was unsaturated, with five-, four-, or three-coordinates in different surfaces. Undercoordinated Mg cations were exposed on the surface. These cations were deficient in electrons and unstable. The donor can stabilized these cations to decrease their electron deficiency. First, the effects of donors on the stability of $MgCl_2$ surfaces were studied using sets of different α-$MgCl_2$ surface period models in Dmol^3 using LDA-PWC. To verify the result of period models, the bulk of α-$MgCl_2$ was calculated by Gaussian 03 using 6-31G(d,p) basis set. 1, 3-dimethoxy-2, 2-dimethylpropane was used as a donor, with saturation of coordinative vacancies. One donor covered the surface (110), and (100) surface with mono-coordination. The bulk of the surface (110) and (100) in the α-$MgCl_2$ all included $(MgCl_2)_9$, while the bulk of the surface (110), (100) and (104) in the β-$MgCl_2$ included 9, 8, and 9 units of $MgCl_2$. The adsorption energies for these complexes were calculated. Table 1 showed the result of LDA-PWC was consistent with that of 6-31G (d,p). Hence, LDA-PWC was adopted to improve the computational efficiency in different $MgCl_2$ surface period models.

3.2 α-$MgCl_2$/Donor Interactions.

A number of computational modeling studies involving α-$MgCl_2$ can be found in the previous literature. Mauro Causà *et al.* [11] used periodic calculations in combination with the dispersion forces to study the bulk and surface structure. The (110) and (100) cuts in α-$MgCl_2$ were the common surface [31]. So in this paper, (110) and (100) surfaces were adopted. The 1,3-dimethoxy-2,2-dimethylpropane (DMDP), and dimethyl phthalate (DMP) were selected as internal electron donor, while dimethoxydimethylsilane (DMDS) was used as external electron donor. DMDP, DMDS and DMP can be bound to the surface of Mg cations because present two

nucleophilic centers-methyl. These donors performed an important function in the Z-N catalyst system: they were used to adjust activities, isotacticity, molecular weights, and molecular weight distributions. Acting as a donor, DMDP, DMDS and DMP affected the electronegativity of Mg and Ti cations in Z-N catalysts. As the molecular-level mechanism of DMDP, DMDS and DMP bound to the $MgCl_2$ surface remains unclear, this topic was studied using a first-principles approach. To determine the influence of $MgCl_2$ surface relaxation on the structure of DMDP, DMDS and DMP surface species, periodic approaches for modeling $MgCl_2$ surface were employed. First, we considered DMDP, DMDS or DMP adsorption on the (110) $MgCl_2$ surface within four approaches: mono-coordination (Figures $3a_1$, b_1 and c_1), bridge coordination (Figures $3a_2$, b_2 and c_2), chelate coordination (Figures $3a_3$, b_3 and c_3), and zip coordination (Figures $3a_4$, b_4 and c_4). The calculated structures of these complexes and the relaxed (110) $MgCl_2$ surface were presented in Figure 3. The adsorption energies, and some interatomic distances for these complexes were elaborated in Table 2. The adsorption energies were about -1.3～-1.6 eV in DMDP/(110) $MgCl_2$ complex, -1.1～-1.3 eV in DMDS/(110) $MgCl_2$ complex and -1.3～-1.8 eV in DMP/(110) $MgCl_2$ complex, respectively. It showed three donors had all strong interaction with the (110) $MgCl_2$ surface, so the donors were easily inclined to load on the (110) $MgCl_2$ surface. To explore to zip coordination as a possibility, the Gibbs free energies were calculated at 298.15 K in $Dmol^3$ to scale down the obtained vibrational frequencies. The ΔG of three modes were -1.31eV, -0.83eV, and -1.56 eV, respectively. It indicated that the processes in zip coordination were feasible in thermodynamics. The result was consistent with the previous research with different density functional method [23, 26].

On the (100) α-$MgCl_2$ surface, three types of the coordination number were existing. They were six-, five- and tri-coordinate, respectively (Figure 1b). The Mg cations were six-coordinate and fill half of the available octahedral sites in $MgCl_2$ crystal, so five- and tri- coordinate Mg ions were unsaturated. DMDP was coordinated with five- and tri-Mg ion in three approaches, which was mono-coordination (Figure 4 a_1 and b_1), bridge coordination (Figure 4 a_2 and b_2), and chelate coordination (Figure

4 a_3 and b_3). Duo to longer distance of interlayer, the zip coordination was not considered. Meanwhile, DMDS and DMP had the same coordination modes with the (100) α-$MgCl_2$ surface (The optimized structures were tabulated and provided in the Supporting Information in Figure S1 and Figure S2). Table 2 showed the adsorption energies, and some interatomic distances for these complexes. The adsorption energies were about -0.1～-0.3 eV, the distances were more than 4.0 Å. All of the results indicated the weak physical adsorption was only existing DMDP/(100) α-$MgCl_2$ complexes. DMDS/(100) α-$MgCl_2$ and DMP/(100) α-$MgCl_2$ complexes had similar results.

3.3 β-$MgCl_2$/Donor Interactions.

β-$MgCl_2$ was also the most successful matrix for Z–N catalysis, Mg cations on the (110) $MgCl_2$ surface was tetra-coordination. DMDP, DMDS or DMP adsorption on the (110) $MgCl_2$ surface took place in four approaches, which was similar to α-$MgCl_2$. The calculated structures of these complexes and the relaxed (110) $MgCl_2$ surface were presented in Supporting Information (Figure S3). The adsorption energies, and some interatomic distances for these complexes were elaborated in Table 3. The bidentate structure was more stable than the mono-dentate structure because the former can provide more electrons to Mg cations than the latter. The adsorption energy was positive in the mono- and bridge coordination modes of DMDP/$MgCl_2$ (110) systems, which indicated that two structures of the complex caused the repulsion between DMDP and $MgCl_2$ (110). The chelate and zip coordination modes presented very large negative adsorption energies, which indicated the complexes were very stable. Moreover, the DMP/ $MgCl_2$ (110) system had a contrary result. The adsorption energies of all modes were more than 0.21 eV, which showde the DMP can't load on the β-$MgCl_2$ (110). In the same study strategy, the DMDS/$MgCl_2$ (110) system was optimized and excellent results (i.e., large absorption energies) were obtained. The adsorption energies of the four modes were more than -1.5 eV. These findings reflected very strong interaction between DMDS and $MgCl_2$ (110). The Gibbs free energies of DMDP/$MgCl_2$ (110) and DMDS/$MgCl_2$ (110) were calculated to explore to zip coordination as a possibility, they were -2.01

eV and -1.82 eV. So DMDP and DMDS easily loaded on the (110) $MgCl_2$ surface in zip coordination.

The interaction between DMDP, DMDS or DMP and $MgCl_2$ (100), which was very important in the Z-N catalyst, was also considered. $MgCl_2$ (100) and $MgCl_2$ (110) shared similar layer-by-layer structures. It had also four approaches like donors/$MgCl_2$ (110) complexes (Figure S4). On the $MgCl_2$ (100) surface, Mg cations were relatively unstable because of tri-coordination. In theory, the interactions between the $MgCl_2$ (100) surface and DMDP, DMDS or DMP were strong because the Mg cations presented an intensely electrophilic center. Table 3 showed that the adsorption energies of the complexes ranged from about -0.6 eV to -0.7 eV in DMDP, from -0.29 eV to -0.35 eV in DMDS, and from 0.5 eV to 0.8 eV in DMP. In fact, compared with the $MgCl_2$ (110) surface, regardless of the donor, the absorption energy of the complexes was very small and may be attributed to only van der Waals forces. Particularly, the absorption energy in DMP/$MgCl_2$ (100) surface was positive, but also the value was huge in all of the systems. This finding may be explained by the steric hindrance presented by methoxyl groups from the donor: H atoms of the methoxyl group and Cl atoms of the $MgCl_2$ (100) surface crowded each other upon attachment of the oxygen atom of the donor to the Mg ions in $MgCl_2$ (100). As such, the distance of Mg-O was about 5 Å at any position of DMDP and the complex obtained from their reaction showed weak interaction. The DMP represented a strange phenomenon, the adsorption energies were more than 0.50 eV whether the distance of Mg-O is 1.91 Å or 4.30 Å. When the donor was DMDS, the distance of Mg-O was 2.53 Å in mono-coordination mode but the absorption energy was only -0.35 eV, which indicated the bond was also weak. Other complexes revealed low absorption energies and longer bonds. In a word, the process that donors absorbed on β-$MgCl_2$ (100) was difficult.

The interactions between DMDP, DMDS and DMP and $MgCl_2$ (104) were finally studied. The interlayer distance in this system was wider than that in other systems, and several Mg atoms were unsaturated on the $MgCl_2$ (104) surface. Therefore, zip coordination mode with the donors was non-existent. The donors

connected to the $MgCl_2$ (104) surface by three approaches: mono-coordination (Figures $5a_1$, b_1, c_1), bridge coordination (Figures $5a_2$, b_2, c_2), and chelate coordination (Figures $5a_3$, b_3, c_3). Table 3 showed that the distance of Mg-O was fairly wide and absorption energies were low or positive when the donor is DMDP, DMP or DMDS. The results obtained were similar to those observed from interactions with the $MgCl_2$ (100) surface and indicated that only van der Waals forces existed in the complexes.

3.4 The effect of coverage

Donor coverage was an important factor that controls the relative stability of $MgCl_2$ surfaces with an effect on $TiCl_4$ adsorption. Considering these aspects, different coverages for three surfaces were modeled using DMDP, DMDS and DMP as the donor. An unsaturated Mg cation on the surface of $MgCl_2$ was considered a vacancy in this study. Only one vacancy was presumed to coordinate a methoxyl of the donor. The coverage function θ was defined as the ratio between the number of donor adsorbed and the number of Mg vacancies on the surface (Equation 2).

$$\theta = \frac{2n_{donor}}{n_{vacancy}} \quad (2)$$

The average donor adsorption energy E_{ad} was calculated based on Equation 3:

$$E_{ad} = \frac{E_{MgCl_2/donor} - E_{MgCl_2} - nE_{donor}}{n} \quad (3)$$

where $E_{MgCl_2/donor}$ was the energy of the system, which was composed of methanol molecule adsorbed on the $MgCl_2$ surface; E_{MgCl_2} and E_{donor} were the energies of the uncovered $MgCl_2$ system and donor in the cell, respectively; and n was the number of adsorbed donor molecules.

In the surface of α-$MgCl_2$, (110) surface was inclined to attach the donor. The coverage of DMDP, DMDS and DMP on the $MgCl_2$ (110) surface in zip coordination were studied. The average donor adsorption energy and distance were calculated. The adsorption energies were calculated to explore the stability of $MgCl_2$ surfaces by donor. Fig. 6a showed that the average E_{ad} was strongly dependent on the coverage of donor on the α-$MgCl_2$ surface. The value of $<d_{Mg-O}>$ was defined by the average value

of all the distances. Fig. 6b showed $<d_{Mg-O}>$ in different coverages, consistent with the adsorption energies. Donors exhibited staggered rivets in the $MgCl_2$ (110) layers. The donors could reject each other when the coverage was increasing, and then the average E_{ad} was decreasing; $<d_{Mg-O}>$ was increasing.

3.5 The mechansim of stereoselectivity.

A typical Z-N catalyst was prepared by treating $MgCl_2$ (or a precursor such as $MgCl_2 \cdot nROH$, $Mg(OR)_2$, and RMgCl) with excess $TiCl_4$ in the presence of a suitable Lewis base (ID), removing the excess of $TiCl_4$, and then activating the catalyst in situ with a mixture of an aluminium trialkyl and a second Lewis base (ED) in the catalyst for propylene polymerization[32, 33]. The role of the internal and external donor in Z-N catalyst was confused. This paper attempted to gain insight into the relation between structural features and stereoselectivity. The process of DMDP, DMDS, and DMP absorption onto the $MgCl_2$ surface was studied by periodic DFT. During the synthesis of Z-N catalysts, the donor connected to the $MgCl_2$ surface, after which $TiCl_4$ exchanged with the donor on the $MgCl_2$ surface (Scheme 1). Table 2 and 3 showed that forces between the donor and the $MgCl_2$ (110) surface were strongest in our study system; thus, the donor can't exchange with $TiCl_4$. $TiCl_4$ can only take the place of donors on $MgCl_2$ (100) or (104) surfaces, consistent with previous experiments [15]. The Ti on the $MgCl_2$ (100) or (104) surface was the isotactic activity center of the molecule, while the one on the (110) surface presented a random character. The donor occupied the (110) surface, and Ti took the place of the (100) or (104) surface. Therefore, polypropylene with high isotacticity can be produced by Z-N catalyst using a donor. In fact, most industry catalysts mainly composed of δ-$MgCl_2$, which has been found to be more efficient. δ-$MgCl_2$ crystal had the statistical stacking sequence of the structural layers, leading to a loss of periodicity in one dimension, which was the mixed crystal of α- and β-$MgCl_2$ [11]. To be more efficient, δ-$MgCl_2$ isn't considered in this paper.

4 Conclusion

The functions of donors on the $MgCl_2$ surface were studied by periodic DFT. Here,

DMDP, DMP, and DMDS were used as donors. Four status aborted on α-$MgCl_2$ (110), (100), and β-$MgCl_2$ (110), (100), and (104) surfaces were considered in different connection modes. Donors on α or β-$MgCl_2$ (110) surface presented the largest absorption energies among all of the complexes studied. Results indicated that the surface of $MgCl_2$ was controlled by choosing an appropriate choice of electron donor. This study provided a sound crystallographic background for Z–N catalysts. The surface of $MgCl_2$ influenced the activity and stereoselectivity of Z–N catalysts. Hence, the theoretical model provided insight into the relationships between the surface and catalytic properties in the catalyst system. Future studies should explore the mechanism of Z–N catalysts using QM.

Supplementary data

The figures of the optimized structures of 1, 3-dimethoxy-2, 2-dimethylpropane, dimethoxy-dimethylsilane, and dimethyl phthalate coordinated the α-$MgCl_2$ (110), (100), and β-$MgCl_2$ (110), (100), and (104) surface in different modes were available.

References

[1] T. Wondimagegn and T. Ziegler, J. Phys. Chem. C, 2012, 116, 1027-1033.

[2] G. Morini, E. Albizzati, G. Balbontin, I. Mingozzi, M. C. Sacchi, F. Forlini and I. Tritto, Macromolecules, 1996, 29, 5770-5776.

[3] V. Busico, J. C. Chadwick, R. Cipullo, S. Ronca and G. Talarico, Macromolecules, 2004, 37, 7437-7443.

[4] B. Liu, T. Nitta, H. Nakatani and M. Terano, Macromol. Chem. Phys., 2003, 204, 395-402.

[5] H. Matsuoka, B. Liu, H. Nakatani and M. Terano, Macromol. Rapid Commun., 2001, 22, 326-328.

[6] E. P. Moore, Jr in Polypropylene Handbook, Hanser Publishers, New York, 1996, Chapter 2, pp 1213.

[7] M. Gao and H. Li, Petrochem. Technol., 2007, 36, 535-546.

[8] W. Kaminsky, Polyolefin: 50 years after Ziegler and Natta I-Polyethylene and Polypropylene, Springer-Verlag Berlin Heidelberg, 2013.

[9] K. Seenivasan, A. Sommazzi, F. Bonino, S. Bordiga and E. Groppo, Chem. Eur. J., 2011, 17, 8648-8656.

[10] V. Busico, M. Causà, R. Cipullo, R. Credendino, F. Cutillo, N. Friederichs, R. Lamanna, A. Segre and V. Van Axel Castelli, J. Phys. Chem. C, 2008, 112, 1081-1089.

[11] R. Credendino, V. Busico, M. Causà, V. Barone, P. H. M. Budzelaar and C. Z. Wilson, Phys. Chem. Chem. Phys., 2009, 11, 6525-6532.

[12] A. Bazhenov, M. Linnolahti, A. J. Karttunen, T. A. Pakkanen, P. Denifl, and T. Leinonen, J. Phys. Chem. C, 2012, 116, 7957-7961.

[13] N. Kashiwa, J. Polym. Sci. A: Polym. Chem., 2004, 42, 1-8.

[14] D. A. Trubitsyn, V. A. Zakharov and I. I. Zakharov, J. Mol. Catal. A: Chem., 2007, 270, 164-170.

[15] A. Turunena, M. Linnolahtia, V. A. Karttunena, T. A. Pakkanena, P. Deniflb and T. Leinonenb, J. Mol. Catal. A: Chem., 2011, 334, 103-107.

[16] J. W. Lee and W. H. Jo, J. Organomet. Chem., 2009, 694, 3076-3083.

[17] M. Seth and T. Ziegler, Macromolecules, 2003, 36, 6613-6623.

[18] Z. Flisak, Macromolecules, 2008, 41, 6920-6924.

[19] T. Wada, T. Taniike, I. Kouzai, S. Takahashi and M. Terano, Macromol. Rapid Commun., 2009, 30, 887-891.

[20] S. Mukhopadhyay, S.A. Kulkarni and S. Bhaduri, J. Mol. Struct., 2004, 673, 65-77.

[21] S. Mukhopadhyay, S. A. Kulkarni and S. Bhaduri, J. Organomet. Chem., 2005, 690, 1356-1365.

[22] L. Cavallo, S. D. Piero, J. Ducèrè, R. Fedele, A. Melchior, G. Morini, F. Piemontesi and M. Tolazzi, J. Phys. Chem. C, 2007, 111, 4412-4419.

[23] K. Vanka, G. Singh, D. Iyer and V. K. Gupta, J. Phys. Chem. C, 2010, 114, 15771-15781.

[24] A. Correa, R. Credendino, J. T. M. Pater, G. Morini and L. Cavallo, Macromolecules, 2012, 45, 3695-3701.

[25] M. Boero, M. Parrinello and K. Terakura, J. Am. Chem. Soc., 1998,120, 2746-2752.

[26] F. Capone, L. Rongo, M. D'Amore, P. H. M. Budzelaar, and V. Busico, J. Phys. Chem. C 2013, 117, 24345−24353

[27] B. Delley, J. Chem. Phys., 1990, 92, 508-517.

[28] B. Delley, J. Chem. Phys., 2000, 113, 7756-7764.

[29] J. P. Perdew and Y. Wang, Phys. Rev. B, 1992, 45, 13244-13249.

[30] H. J. Monkhorst and J. D. Pack, Phys. Rev. B, 1976, 13, 5188-5192.

[31] L. Brambilla, G. Zerbi, F. Piemontesi, S. Nascetti and G. Morini, J. Mol. Catal. A: Chem., 2007, 263, 103-111.

[32] S. Tanase, K. Katayama, S. Inasawa, F. Okada, Y. Yamaguchi, T. Konakazawa, T. Junke and N. Ishihara, Appl. Catal. A: Gen., 2008, 350, 197-206.

[33] Y. Ling, W. Chen, L. Xie, Y. Liu and G. Zheng, J. Appl. Polym. Sci., 2008, 110, 3448-3454.

Fig. 1 The α-$MgCl_2$(110) (a), α-$MgCl_2$(110) (b), β-$MgCl_2$(110) (c), β-$MgCl_2$(100) (d), and β-$MgCl_2$(104) (e) modes. Green balls indicate Cl atoms while violet bars indicate Mg atoms.

Fig. 2 Structural formulas and ball-stick modes of 1,3-dimethoxy-2,2-dimethylpropane (a_1, a_2), dimethoxydimethylsilane (b_1, b_2) and dimethyl phthalate (c_1,c_2).

Fig. 3 Optimized structures of DMDP, DMDS, and DMP complexes in α-$MgCl_2$ (110): Mono-coordination (a_1.b_1, c_1), bridge coordination (a_2.b_2, c_2), chelate coordination (a_3.b_3, c_3), and zip coordination (a_4.b_4, c_4) modes.

Fig. 4 Optimized structures of DMDP/α-$MgCl_2$ (100) complexes, $a_{1\sim3}$ is tri-coordinate, $b_{1\sim3}$ is five-coordinate.

Fig. 5 Optimized structures of DMDP/β-$MgCl_2$ (104) ($a_{1\sim3}$), DMDS/β-$MgCl_2$ (104) ($b_{1\sim3}$) and DMP/$MgCl_2$ (104) ($c_{1\sim3}$) complexes.

Fig. 6. The average energy of three donors adsorption (a) and average distance of Mg–O (b) in the (110) surfaces of α-$MgCl_2$.

Scheme 1. Process of supporting $TiCl_4$ on the $MgCl_2$ surface.

Table 1. Absorption energy (eV) of 1, 3-dimethoxy-2, 2-dimethylpropane on the surface of $MgCl_2$

Table 2. Absorption energy and distance of Mg-O in α-$MgCl_2$.

Table 3. Absorption energy and distance of Mg-O in β-$MgCl_2$.

Table 1. Absorption energy (eV) of 1, 3-dimethoxy-2, 2-dimethylpropane on the surface of $MgCl_2$

	α-$MgCl_2$		β-$MgCl_2$		
	110	100	110	100	104
LDA-PWC	-1.53	-0.21	0.78	-0.65	-0.65
6-31G(d,p)	-1.83	-0.26	0.82	-0.69	-0.71

Table 2. Absorption energy and distance of Mg-O in α-$MgCl_2$

	ΔE/ev	d_1/Å	d_2/Å		ΔE/ev	d_1/Å	d_2/Å		ΔE/ev	d_1/Å	d_2/Å
	DMDP				DMDS				DMP		
110											
a_1	-1.53	3.93		b_1	-1.28	2.41		c_1	-1.62	2.02	
a_2	-1.33	4.42	4.93	b_2	-1.25	3.50	4.72	c_2	-1.83	2.01	2.03
a_3	-1.58	3.87	3.88	b_3	-1.18	4.12	4.90	c_3	-1.85	3.91	4.62
a_4	-1.36	4.21	4.73	b_4	-1.15	4.42	5.13	c_4	-1.38	3.78	3.81
100											
a_1	-0.21	4.20		a_1	-0.006	4.01		a_1	-0.21	4.52	
a_2	-0.15	4.31	4.19	a_2	0.055	4.91	6.01	a_2	-0.18	4.80	5.12
a_3	-0.28	4.71	4.60	a_3	0.062	4.83	5.46	a_3	-0.17	5.06	5.38
b_1	-0.21	4.92		b_1	0.121	3.85		b_1	-0.13	5.21	
b_2	-0.22	4.95	5.21	b_2	0.078	4.720	5.02	b_2	-0.15	5.22	5.64
b_3	-0.20	5.23	5.35	b_3	0.052	5.93	5.52	b_3	-0.15	5.43	5.22

Table 3. Absorption energy and distance of Mg-O in β-$MgCl_2$

	ΔE/ev	d_1/Å	d_2/Å		ΔE/ev	d_1/Å	d_2/Å		ΔE/ev	d_1/Å	d_2/Å
	DMDP				DMDS				DMP		
110											
a_1	0.78	4.51		b_1	-1.75	2.35		c_1	0.26	2.83	
a_2	0.76	4.32	4.99	b_2	-1.56	4.81	5.83	c_2	0.44	4.01	4.65
a_3	-1.96	4.41	4.46	b_3	-1.61	3.52	4.90	c_3	0.21	2.50	3.62
a_4	-1.98	4.82	4.90	b_4	-1.79	4.61	5.43	c_4	0.41	4.01	4.43
100											
a_1	-0.65	4.90		b_1	-0.35	2.53		c_1	0.62	1.91	
a_2	-0.71	4.92	4.93	b_2	-0.29	3.71	4.94	c_2	0.81	1.92	1.96
a_3	-0.70	5.19	5.16	b_3	-0.30	3.81	4.93	c_3	0.54	2.30	2.29
a_4	-0.68	5.01	5.18	b_4	-0.31	3.81	5.52	c_4	0.75	3.91	4.30
104											
a_1	-0.65	3.95		b_1	-0.22	3.82		c_1	0.23	2.02	
a_2	-0.69	4.13	4.15	b_2	-0.27	3.43	4.95	c_2	0.76	2.00	1.98
a_3	-0.72	3.91	4.32	b_3	-0.29	3.62	3.54	c_3	0.57	2.00	2.02

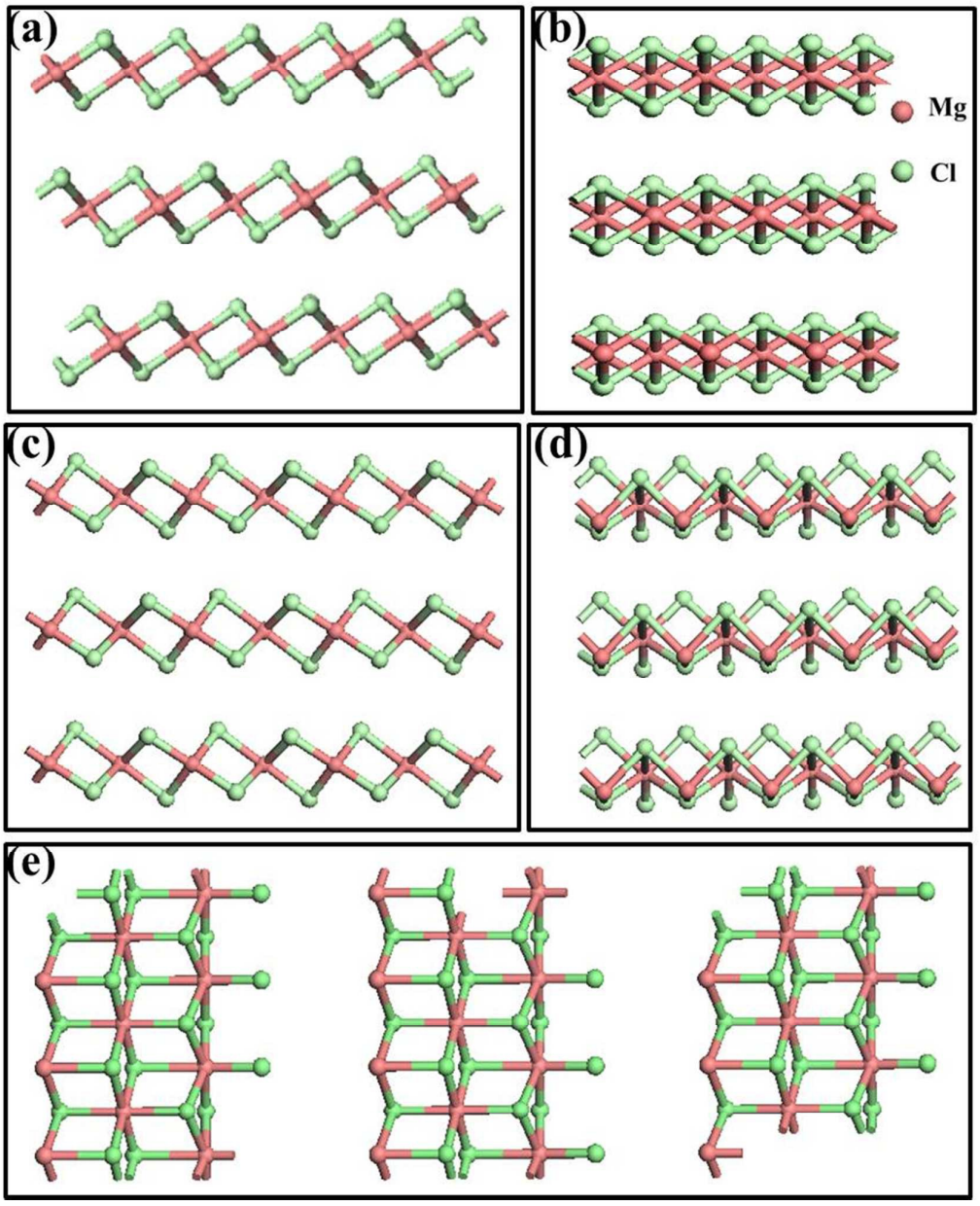

Fig. 1 The α-$MgCl_2$(110) (a), α-$MgCl_2$(110) (b), β-$MgCl_2$(110) (c), β-$MgCl_2$(100) (d), and β-$MgCl_2$(104) (e) modes. Green balls indicate Cl atoms while violet bars indicate Mg atoms.

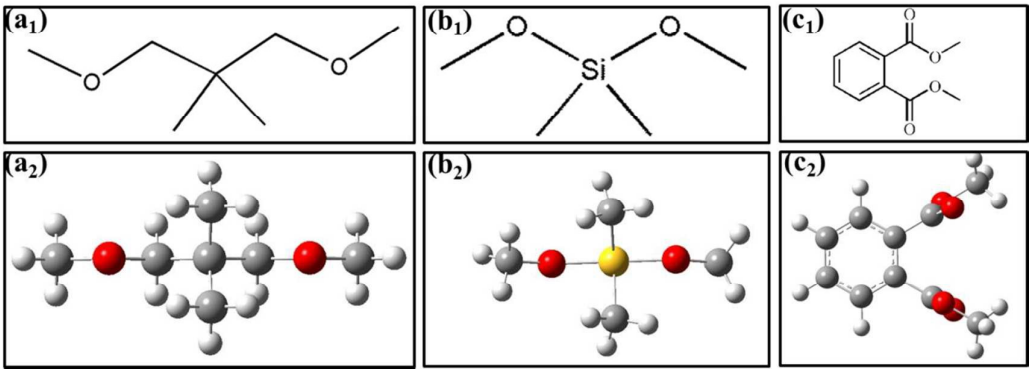

Fig. 2 Structural formulas and ball-stick modes of 1,3-dimethoxy-2,2-dimethylpropane (a_1, a_2), dimethoxydimethylsilane (b_1, b_2) and dimethyl phthalate (c_1,c_2).

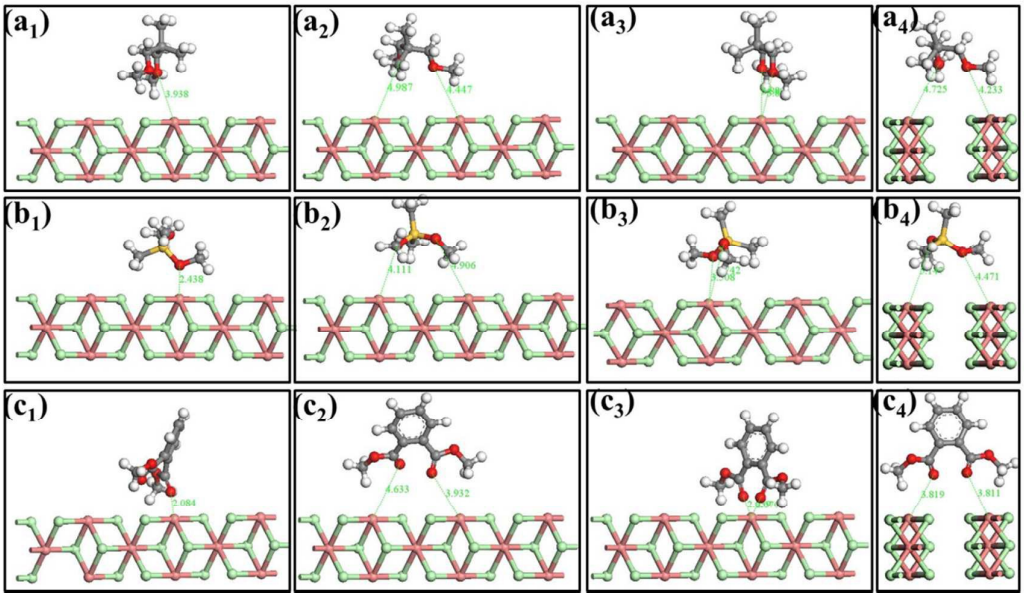

Fig. 3 Optimized structures of DMDP, DMDS, and DMP complexes in α-$MgCl_2$ (110): Mono-coordination (a_1.b_1, c_1), bridge coordination (a_2.b_2, c_2), chelate coordination (a_3.b_3, c_3), and zip coordination (a_4.b_4, c_4) modes.

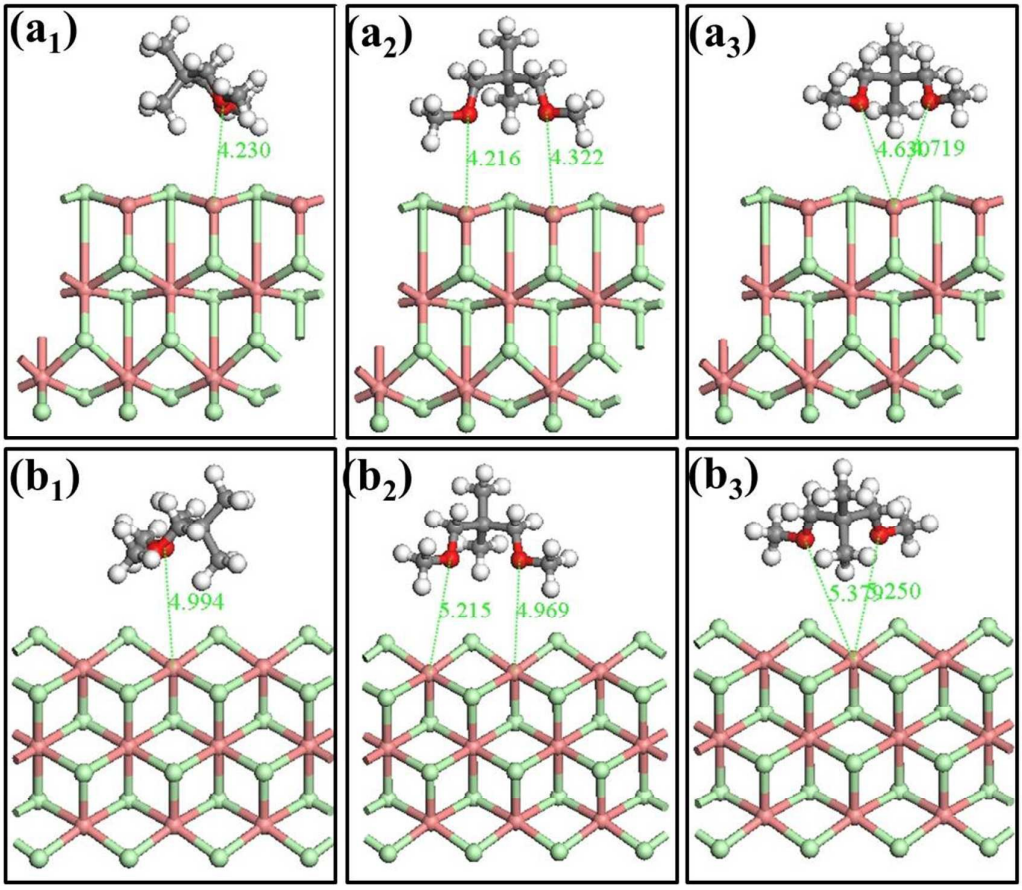

Fig. 4 Optimized structures of DMDP/α-$MgCl_2$ (100) complexes, $a_{1\sim3}$ is tri-coordinate, $b_{1\sim3}$ is five-coordinate.

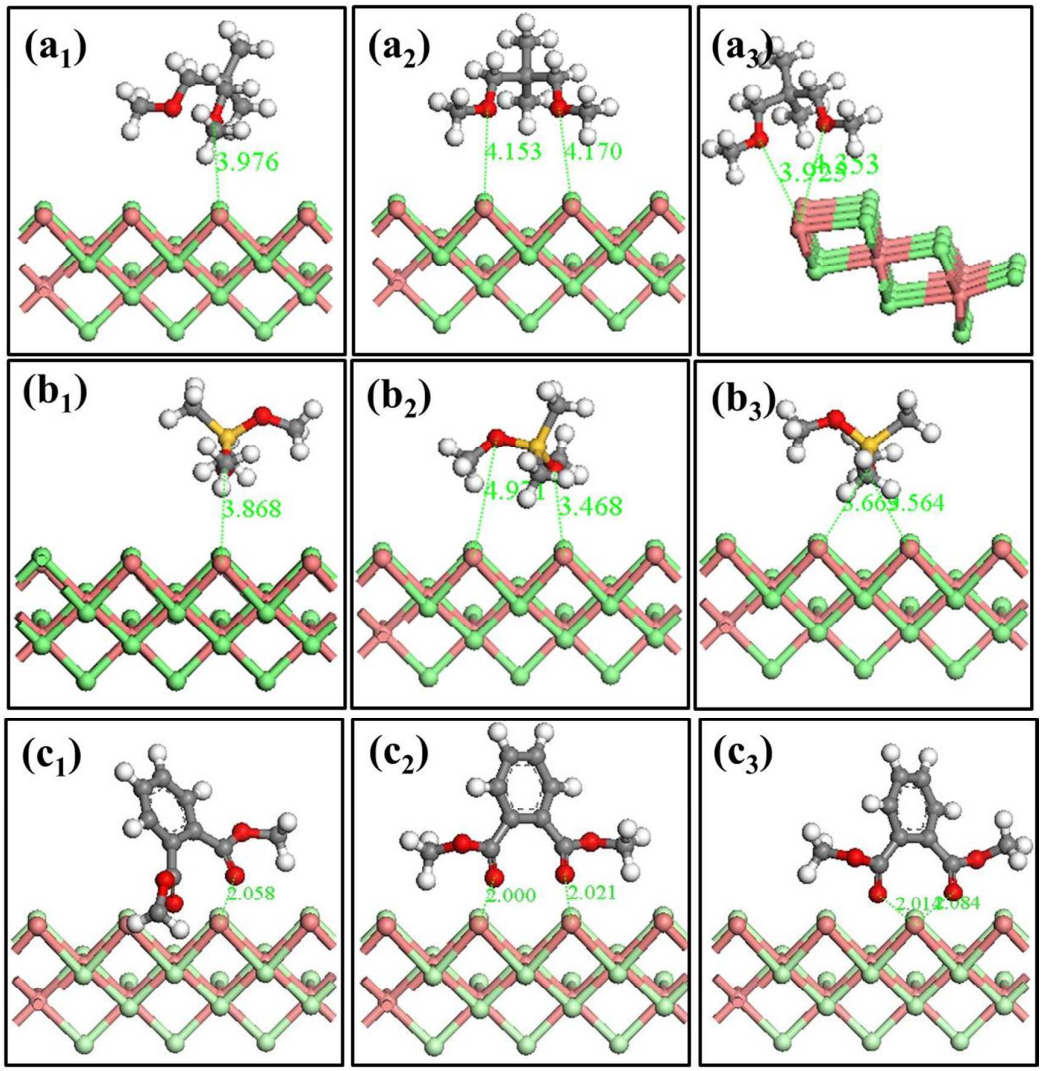

Fig. 5 Optimized structures of DMDP/β-$MgCl_2$ (104) ($a_{1\sim3}$), DMDS/β-$MgCl_2$ (104) ($b_{1\sim3}$) and DMP/$MgCl_2$ (104) ($c_{1\sim3}$) complexes.

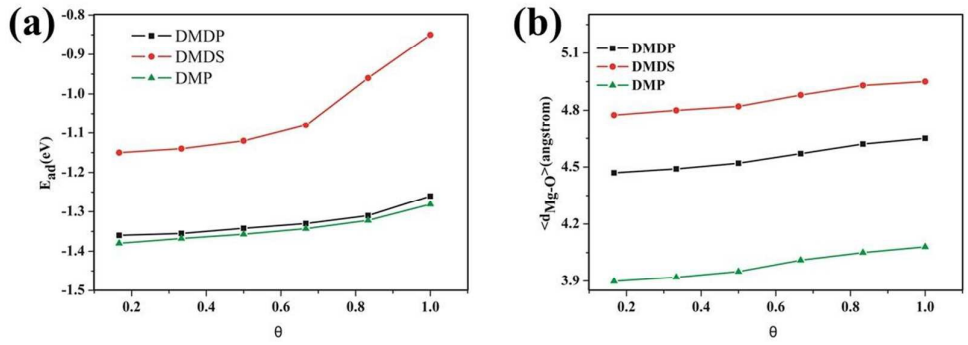

Fig. 6. The average energy of three donors adsorption (a) and average distance of Mg–O (b) in the (110) surfaces of α-$MgCl_2$.

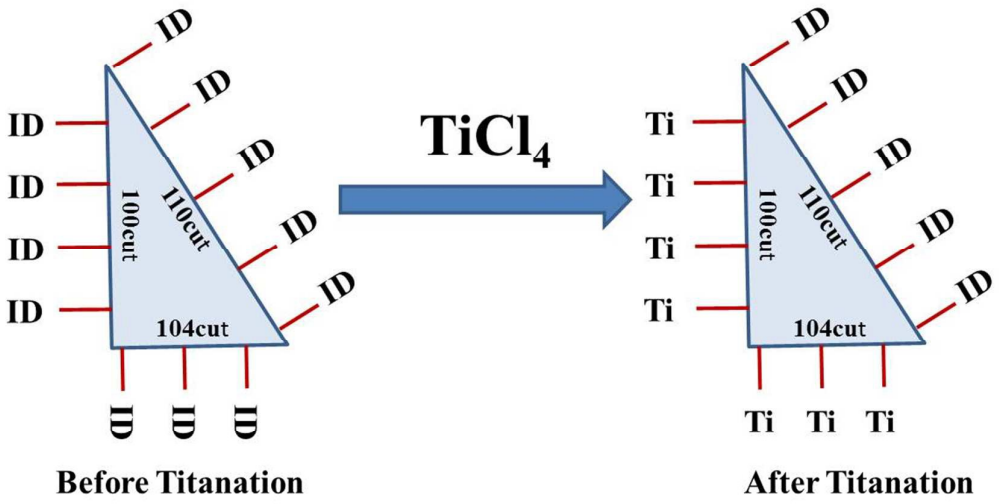

Scheme 1. Process of supporting $TiCl_4$ on the $MgCl_2$ surface.

Periodic DFT Study of the Donor Interactions with the $MgCl_2$ Surface in the Ziegler-Natta Catalytic System

Kefeng Xie[a,b], Bochao Zhu[b], Renwei Xu[b], Jingcheng Xu[c], Peng Liu[a,*]

[a]College of Chemistry and Chemical Engineering, Lanzhou University, Lanzhou, 730000, China

[b]Lanzhou Petrochemical Research Center, Petrochina, Lanzhou, 730060, China

[c]School of Materials Science and Engineering, University of Shanghai for Science and Technology, Shanghai, 200093, China

Email: pliu@lzu.edu.cn